

Forced response of the El Niño–Southern Oscillation–Indian monsoon teleconnection in the MPI-GE

Tamás Bódai^{1,2}, Gábor Drótos³, Tímea Haszpra⁴

¹Center for Climate Physics, Institute for Basic Science, Korea, ²Pusan National University, ³Instituto de Física Interdisciplinar y Sistemas Complejos, ⁴Eötvös University Budapest



- The ENSO has a global reach in shaping local weather, but affects tropical and subtropical regions the most [1].
- The teleconnection of the ENSO with the Asian monsoon systems has the greatest impact on human life, and severe episodes in the late XIX. century lead to the discovery of the ENSO [2].
- The ENSO-Indian monsoon (IM) teleconnection seems to have been weakening in the recent decades in the view of running correlations [3].
- However, not necessarily as a contradiction, the MPI-GE [4] was found recently [5] to feature a strengthening of the ENSO-IM teleconnection in a correct ensemble-based framework [6].
- Although certain discrepancies between the analysed representations of the ENSO-IM teleconnection exist [6] (Figs. 2, 3).
- OBJECTIVE: Here we aim to examine the robustness of the forced change of the relationship by
 - Separating spatial characteristics via using the snapshot EOF analysis [7], Maximum Covariance Analysis (MCA) and Canonical Correlation Analysis (CCA); and
 - Decomposing the forced change of the correlation coefficient, in terms of a regression model, into three components.

Methodology

- In our original approach [6], we represented the Indian summer monsoon rain (ISMR) by the JJAS total precipitation P over India, and the ENSO by the JJA average surface pressure difference p_{diff} between Tahiti and Darwin or the average sea surface temperature T in a “Nino box”.
- Here, instead of e.g. spatial averages, we project the full (JJA mean) fields of P , p , T onto dominant modes of variability, be it an EOF, or dominant modes concerning, specifically, the ENSO-IM relationship.
- We define the teleconnection as the Pearson’s correlation coefficient between scalars; e.g.:

$$r = \frac{\langle p_{diff} P \rangle - \langle p_{diff} \rangle \langle P \rangle}{\sqrt{(\langle p_{diff}^2 \rangle - \langle p_{diff} \rangle^2)(\langle P^2 \rangle - \langle P \rangle^2)}}$$

- or between PCs belonging to the EOF/MCA/CCA modes,
- but we average $\langle \rangle$ over the ensemble members instead of time.
- Due to the *finite* ensemble size N , fine details of the response are masked by “noise”, and even the nonstationarity is hard to see/detect. To this end, as a quantitative strategy, we deploy the Mann-Kendall (MK) test to detect nonstationarity in the *Fisher transform* $z = \arctan(r)$, which follows approximately a *normal* distribution of standard deviation $(N - 3)^{-1/2}$.
- In terms of the linear regression model $\Psi = \alpha\Phi + \xi$, the correlation coefficient can be written as:

$$r = \frac{1}{\sqrt{1 + \left(\frac{\sigma_{\xi}/\alpha}{\sigma_{\Phi}}\right)^2}}$$

- To attribute temporal forced changes of the ensemble-wise r , we evaluate the time series of the ensemble-wise
 - ENSO variability σ_{Φ} ;
 - ENSO-IM “coupling” α being the regression coefficient;
 - Noise strength σ_{ξ} .

Findings

- No changes of EOF, MCA, CCA modes on the ENSO side (Fig. 1a); some change in the late 21st c. under RCP8.5 on the IM side (Fig. 1b).
- A robust picture of **long-term strengthening** of the ENSO-IM teleconnection wrt. the most dominant (first) EOF/MCA/CCA modes.
- Although the **strengthening is declining**. In the 21st c. alone typically no significant change can be detected, only in the 20th c., but as the 20th c. period is extended steadily into the future, the test statistics is typically steadily increasing, hinting at a continued increase of r (Fig. 3).
- As for the drivers (Fig. 2),
 - Up to a point in time, ENSO variability typically increases (SST) or stagnates (SLP); +ve or no contribution;
 - The coupling is typically strengthening throughout: +ve contribution;
 - The noise strength is typically increasing throughout: –ve contribution.
- Both an increasing ENSO variability (1.) and the remaining two factors (2. and 3.) combined can contribute to an increase of r . That is, the strengthening coupling typically dominates over an increasing noise strength.
- ENSO variability declines in the second half of the 21st c., upon a seemingly abrupt turn of the trend.
- This decline can make r decline too, although this effect can be muffed by the accelerating change in the other factors.

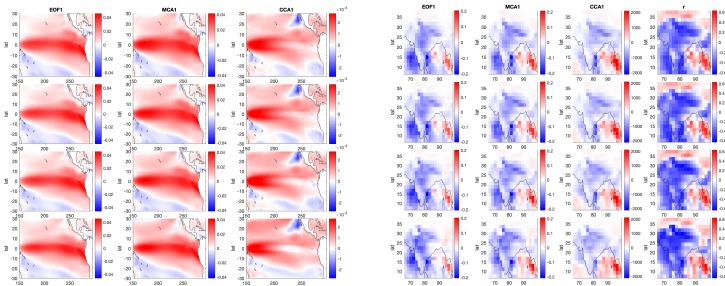


Figure 1. Temporal-mean 1st EOF (left), MCA (middle), CCA (right) modes in four (rows) consecutive 50 year time windows starting from 1900. (a) ENSO, characterised by SST; (b) Indian monsoon. For (b), we also have correlation maps: the corr’ coeff’ between the gridpoint-wise precipitation and PC1 of EOF1.

Figure 2. Time series of the ensemble-wise correlation coefficients r between scalar time series e.g. Nino3 and ISMR, or PCs of EOFs or those of MCA and CCA modes (one column for each). Below each $r(t)$ are corresponding time series for ENSO variability σ_{Φ} , ENSO-IM coupling/reg’ coeff α , noise strength σ_{ξ} . On the left (right) ENSO characterisation is based on the SST (SLP).

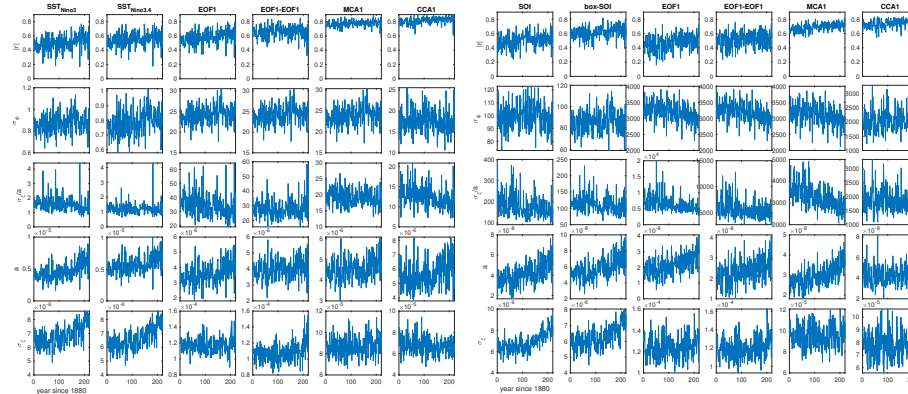
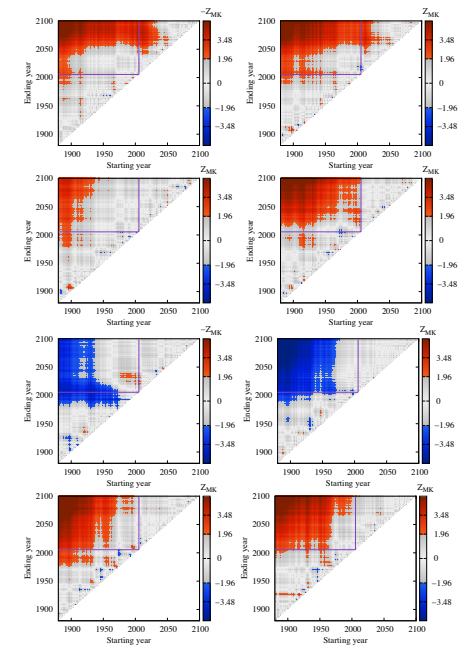


Figure 3. Mann-Kendall test statistics based on some of the $r(t)$ seen in Fig. 2. Top (bottom) block of four is based on the SST (SLP).



[1] Neelin, J. D. et al. (1998) J. Geophys. Res. Ocean. 103, 14261–14290. [2] Mike Davies. Late Victorian Holocaust. Verso (2000). [3] Kumar, K.K. et al. (1999) Science 284:2156–2159. [4] Maher, N. et al. (2019) JAMES, 11(7):2050–2069. [5] Bódai, T. et al. (2020) J. Clim. 33(6):2163–2182. [6] Tel, T. et al. (2020) J. Stat. Phys. doi.org/10.1007/s10955-019-02445-7 [7] Haszpra, T. et al. (2020) ESD 11(1): 267–280.